PNAS
www.pnas.org

Supplementary Information for

Structural analysis of the intrinsically disordered splicing factor Spp2 and its binding to the DEAH-box ATPase Prp2

Florian Hamann, Andreas Schmitt, Filippo Favretto, Romina Hofele, Piotr Neumann, ShengQi Xiang, Henning Urlaub, Markus Zweckstetter and Ralf Ficner

Ralf Ficner
Email: rficner@uni-goettingen.de

This PDF file includes:

www.pnas.org/cgi/doi/10.1073/pnas.1907960117

Supplementary Information text

MATERIAL AND METHODS:

Protein expression and purification

For expression of *Saccharomyces cerevisiae* Spp2 (scSpp2), cDNA encoding truncated proteins comprising either residues 10 – 185 or the G-patch containing region 100 – 150 were cloned into pET-21a vector. The recombinant proteins with C-terminal hexa-histidine tag were expressed in *Escherichia coli* Rosetta II (DE3) at 16 °C. Cells were disrupted in 50 mM HEPES/NaOH (pH 7.5), 500 mM NaCl, 5% (v/v) glycerol, 2 mM β-mercaptoethanol and lysate was clarified by centrifugation for 30 minutes at 30,000 xg. The proteins were purified at 20 °C on a Ni-NTA-Sepharose column (in 50 mM HEPES/NaOH (pH 7.5), 500 mM NaCl, 5% (v/v) glycerol, 30 mM imidazole, 2 mM β-mercaptoethanol) including a wash step with binding buffer supplemented with 2 M LiCl to remove bound nucleic acids. The buffer was exchanged against 10 mM HEPES/NaOH (pH 7.5), 50 mM NaCl, 5% (v/v) glycerol, 2 mM β-mercaptoethanol using a HiTrap desalting column (GE Healthcare). Further purification was obtained by anion-exchange chromatography using a Source30Q column. Finally, the protein was purified by a Superdex-75 gelfiltration column (GE Healthcare) in a buffer containing 10 mM HEPES/NaOH (pH 7.5), 100 mM NaCl, 5% (v/v) glycerol, 2 mM β-mercaptoethanol. The protein was concentrated to 10 mg/ml using an Amicon Ultra centrifugal concentrator (Merck) in 10 mM HEPES/NaOH (pH 7.5), 200 mM NaCl, 5% (v/v) glycerol and 2 mM β-mercaptoethanol. For NMR-experiments, $scSpp2_{10-185}$ was expressed in M9 minimal media supplemented with $^{15}NH_4Cl$. Purification of the N15-labeled scSpp2 was performed as described above.

Spp2 from *Chaetomium thermophilum* (ctSpp2) was identified by NCBI BLAST search tool (GenBank: EGS17798.1) and the gene encoding for the full-length protein was amplified by PCR from a total DNA preparation. The PCR product was cloned into the IBA Stargate pASG-IBA-3 vector according to the manufacturer's protocol. The Strep-tagged recombinant protein was expressed in *Escherichia coli* Rosetta II (DE3) at 16°C. Cells were disrupted using a fluidizer (Microfluidics) in 50 mM HEPES/NaOH (pH 7.5), 500 mM NaCl, 5% (v/v) glycerol, 1 mM DTT and lysate was clarified by centrifugation for 30 minutes at 30,000 xg. The protein was purified at 20 °C on a Streptactin-Sepharose column (in 50 mM HEPES/NaOH (pH 7.5), 500 mM NaCl, 5% (v/v) glycerol, 1 mM DTT). Further purification was obtained by a Superdex-75 gelfiltration column. The protein was concentrated to 20 mg/ml in 10 mM HEPES/NaOH (pH 7.5), 150 mM NaCl, and 1 mM DTT.

For expression of truncated ctSpp2 comprising G-patch residues 211 – 254, the encoding gene was amplified by PCR from a total DNA preparation (1). The PCR product was cloned into the IBA Stargate pASG-IBA-25 vector according to the manufacturer's protocol. Expression and purification by Glutathion-Speharose was performed as described for scSpp2. Further purification was achieved by a Superdex-75 gelfiltration column. The protein was concentrated to 20 mg/ml in 10 mM HEPES/NaOH (pH 7.5), 150 mM NaCl, and 1 mM DTT. Mutants of the ctSpp2 G-patch motif were purified as described above.

For NMR studies a construct of the ctSpp2 G-patch comprising residues 208 – 254 was cloned into the plasmid pASG-IBA 25, which was transformed into BL21 (DE3) cells. $ctSpp2_{208-254}$ was expressed in M9 minimal medium for the production of ^{15}N- and ^{15}N, ^{13}C-labelled $ctSpp2_{208-254}$. Purification of this construct was

performed as described for ctSpp2$_{211-254}$, with the exception of the gelfiltration buffer containing 10 mM HEPES/NaOH pH 7.5, 200 mM NaCl, 5% Glycerol, 1 mM DTT and 0.02% NaN_3. Prior to NMR studies the buffer was exchanged to 10 mM HEPES/NaOH pH 6.5, 200 mM NaCl, 0.5% Glycerol, 1 mM DTT, 5 mM EDTA and 0.02% NaN_3, supplemented with 5% of D2O.
ctPrp2 was expressed and purified as described in Schmitt et al. (2018) (2).

Far-UV circular dichroism spectroscopy

scSpp2$_{10-185}$ and scSpp2$_{100-150}$ samples were dialyzed against buffer containing 100 mM sodium phosphate pH 7.5 and diluted to 0.1 mg/ml. ctSpp2$_{208-254}$ was dialyzed in pure water and diluted to a final concentration of 0.2 mg/ml. 200 µL of the sample were pipetted into a cuvette with a path length of 1 mm and transferred into a Chirascan CD spectrometer (AppliedPhotophysics). The spectra were recorded in the far UV range from 190 – 260 nm at 20 °C with a time-per-point value of 1 s and a path length of 1 nm. Every measurement was performed three times. For the final absorption curve, the values of the negative control, which contained exclusively the sample buffer or pure water, were subtracted from the values of the protein sample.

NMR spectroscopy

NMR experiments on scSpp2$_{10-185}$ and scSpp2$_{100-150}$ were measured at 288 K on a Bruker Avance III 600 MHz spectrometers equipped with a TCI cryoprobe. The 2D ^{1}H-^{15}N HSQC was recorded at 288K with 1024(H)*300(N) complex points. Four transients were accumulated for each FID. NMR experiments on ctSpp2$_{208-254}$ were performed on a Bruker Avance III 700 MHz spectrometer equipped with a TCI cryogenic probe. The 2D ^{1}H-^{15}N HSQC of ctSpp2$_{208-254}$ was recorded at 298 K with 2048(H)*256(N) complex points. Eight transients were accumulated for each FID. For backbone resonance assignment, the three-dimensional triple resonance experiments HNCA, HN(CO)CA, HNCACB, CBCA(CO)NH and HNCO (3) were recorded on uniformly ^{15}N,^{13}C-labelled ctSpp2$_{208-254}$ at 298 K with 2048(H)*62(N)*114(C) complex points.

Steady-state heteronuclear {^{1}H,^{15}N}-NOE values were measured at 298 K with two different datasets, one collected without initial proton presaturation and a second with ^{1}H presaturation. The proton saturation period was set to 4 s. Spectra were processed with Topspin (Bruker) and NMRPipe (4) and analyzed with ccpnmr Analysis 2.2.1 (5).
The heteronuclear steady-state {^{1}H,^{15}N}-NOE values were obtained calculating the ratio of peak intensities of the saturated spectrum to the intensities of the unsaturated spectrum.
Errors were estimated by evaluating the standard deviation (SD) of the NOE (σ_{NOE}) calculated as:

$$\sigma_{NOE}/NOE = ((\sigma I_{sat}/I_{sat})^2 + (\sigma I_{unsat}/I_{unsat})^2)^{1/2}$$

where σI_{sat} and σI_{unsat} are the standard deviations of the noise in the spectra.
The conformational sampling and ensemble selection algorithm *flexible-meccano* was used to calculate a statistical ensemble of ctSpp2$_{208-254}$ (6) assuming an α-helical propensity of 20 % for residues F214-S221, which was determined from the experimental $^{13}C\alpha$ and $^{13}C\beta$ chemical shift as described by Marsh et al. (7).

Dynamic light scattering

Dynamic light scattering was performed on a sample of ctSpp2$_{208-254}$ (concentration of 0.2 mM) at 25 °C both in water and in 10 mM HEPES/NaOH pH 6.5, 200 mM NaCl, 0.5% Glycerol, 1 mM DTT, 5 mM EDTA and 0.02% NaN_3. Measurements were acquired in triplicates on a Dynamic proTitan DLS instrument equipped with a temperature control system (Wyatt technology corporation) with a power laser strength of 60%. Samples were allowed to equilibrate for one minute before starting the acquisition.

Crystallization

Crystals of crystal forms 1 – 4 were grown at 20°C by sitting drop vapor diffusion after mixing 1µl of reservoir solution with 1µl of 2.5 mg/ml ctPrp2 supplemented with a 2-fold excess of ctSpp2$_{211-254}$, 10-fold molar excess of ADP, a 20-fold molar excess of $BeSO_4$, a 60-fold molar excess NaF and a 2.5-fold molar excess of U_{12}-RNA (AXOlabs, Germany). Crystals of CF1 were obtained in 100 mM MES pH 6.5, 350 mM calcium acetate and 19% (w/v) PEG4000; crystals of CF2 in 100 mM Bis-Tris pH 5.5, 400 mM ammonium sulfate and 23% (w/v) PEG3350; crystals of CF3 in 100 mM sodium cacodylate pH 6, 33 mM KCl, 12% (v/v) isopropyl alcohol and 25 mM $MgCl_2$ and crystals of CF4 in 100 mM HEPES/NaOH pH 7, 8% (w/v) polyvinyl alcohol and 7.5% (v/v) isopropyl alcohol. Crystals of CF5 were grown at 20°C by sitting drop vapor diffusion after mixing 1µl of reservoir solution with 2µl of 3.5 mg/ml ctPrp2 supplemented with 3-fold molar excess of ctSpp2$_{211-254}$ and a 10-fold molar excess of ADP. CF5 crystals were obtained in 100 mM Bicine/Trizma pH 7.5, 11% (w/v) PEG8000, 20% (w/v) ethylene glycol, 20 mM of a monosaccharide mixture (D-glucose, D-mannose, D-galactose, L-fucose, D-xylose and N-acetyl-D-glucosamine).

Data collection and processing

Crystals of CF1 and CF2 were cryoprotected in the respective reservoir solution complemented with 10% (w/v) glycerol, CF3 with 40% (w/v) glycerol, CF4 with 25% glycerol and CF5 was not additionally cryoprotected. X-ray diffraction data of CF1, CF2 and CF5 were collected at 100 K on beamline P13 and CF3 as well as CF4 were collected at beamline P14, PETRA III, DESY (Hamburg, Germany). Processing of the diffraction data was performed with the XDS package (8). The highest resolution limit was estimated using a minimum I/σ(I) of 1.5 and a minimum $CC_{1/2}$ of 60% as cutting criteria. X-ray diffraction data statistics are summarized in SI Appendix, Table S1.

Structure solution, refinement and analysis

All crystal forms of the ctPrp2-ctSpp2 complex were solved by molecular replacement using *Phaser* with the structure of ctPrp2 (PDBid: 6fa5) as a search model (2, 9). After an initial refinement with *PHENIX*, the ctSpp2 G-patch could be built manually with *Coot* using the mF_o-DF_c map (10, 11). All consecutive refinement cycles were performed with *PHENIX* including TLS, weight optimization and bulk-solvent

optimization. The quality of the final models was assessed *MolProbity* and with the validation tools in *PHENIX* (12). The figures were prepared with PyMOL (v.1.8; Schrödinger).

Protein-protein cross-linking

The optimal cross-linker to protein ratio was determined by using 2.5 µg aliquots of the ctPrp2/ctSpp2 complex and a series of cross-linker molar excesses of 5, 10, 25, 50, 100 and 200 as well as a control. Samples were allowed to react with freshly prepared BS3 for 30 minutes at room temperature. The chosen cross-linker to protein ratio was 75, which led to a high yield, yet to a homogeneous sharp band as visualized on SDS-PAGE. The cross-linked samples were analyzed by SDS page on a 4-12% Bis-Tris gel (Invitrogen) with MES as running buffer and stained with Coomassie blue.

For MS analysis, the ctPrp2/ctSpp2 mixture was cross-linked with freshly prepared BS3 and EDC (Pierce, Thermo Scientific) in a 75:1 cross-linker to protein ratio, allowed to react and separated as described above. Cross-linked bands were excised from the gel and combined in a single reaction cup according to cross-linking reagent. In gel digestion and extraction of peptides was achieved as described elsewhere (13). The solution of extracted peptides was concentrated on a vacuum evaporator to 5 µL and diluted to a final volume of 10 µl to reach a sample solvent composition of 5% (v/v) CAN, 1% (v/v) FA. Samples were submitted for immediate analysis to the mass spectrometer. Mass spectrometric analysis and cross-link identification were performed as described elsewhere (14).

Isothermal titration calorimetry (ITC)

The binding of ADP to ctPrp2 in the presence of $ctSpp2_{211-254}$ was assessed via ITC with a MicroCal VP-ITC (Malvern) using a ctPrp2 and $ctSpp2_{211-254}$ concentration of 10 µM and 20 µM, respectively, in the cell and a concentration of 100 µM ADP in the syringe. A reaction buffer consisting of 20 mM HEPES pH 7.5, 200 mM NaCl, 5% glycerol and 2 mM $MgCl_2$ was used. Each measurement consisted of an initial 6 µl injection and injections with a volume of 14 µl injected with a speed of 1 µl s^{-1}. The interval between each injection was set to 250 s and the binding was monitored at 25°C.

The binding of truncated constructs of $ctSpp2_{G\text{-}patch}$ ($ctSpp2_{G\text{-}patch}\Delta C$, $ctSpp2_{G\text{-}patch}\Delta LC$, $ctSpp2_{G\text{-}patch}\Delta NL$; EMC microcollections) towards ctPrp2 was determined using a MicroCal PEAQ-ITC (Malvern). $ctSpp2_{G\text{-}patch}\Delta C$ consists of residues 211-237, $ctSpp2_{G\text{-}patch}\Delta LC$ of residues 211-229 and $ctSpp2_{G\text{-}patch}\Delta NL$ of residues 238-254.The measurement s were performed using a concentration of 30 µM ctPrp2 in the cell and 300 µM, 350 µM, 600 µM and 700 µM of $ctSpp2_{G\text{-}patch}$, $ctSpp2_{G\text{-}patch}\Delta C$, $ctSpp2_{G\text{-}patch}\Delta LC$, $ctSpp2_{G\text{-}patch}\Delta NL$, respectively, in the syringe. The reaction buffer consisted of 20 mM Tris/HCl pH 7.5, 200 mM NaCl, 5% glycerol and 2 mM $MgCl_2$. Each measurement consisted of an initial 0.8 µl injection and injections of 4 µl injected with a speed of 2 µl s^{-1}. The interval between each injection was set to 250 s and the binding was monitored at 25°C. Due to the low affinity and in order to obtain saturation, consecutive measurements of $ctSpp2_{G\text{-}patch}\Delta C$ and $ctSpp2_{G\text{-}patch}\Delta LC$ with identical settings as described above were performed. All measurements were baseline and offset corrected.

GST pulldown

GST-tagged ctPrp2 and ctSpp2 mutants were purified as already described. 100 µl of GSH-Sepharose beads (GE Healthcare) were equilibrated with buffer A containing 10 mM HEPES/NaOH pH 7.5, 300 mM NaCl, 2 mM MgCl2, 5% glycerol and 1 mM DTT. 2 nmol of GST-ctPrp2 were added to the beads and incubated for 30 minutes at 16°C. The GSH-Sepharose beads were washed 4 times with 8 bed volumes buffer A. 4 nmol ctSpp2 were added, incubated for 30 minutes at 16°C and washed as described before. The bound fraction was eluted by addition of 100 µl buffer A supplemented with 30 mM reduced Glutathione and the samples were analyzed on a 4-20% SDS- PAGE gel (Expedeon).

ATPase activity

The ability of Prp2 to hydrolyze ATP, AMPPNP and ATPγS was assessed using an ATPase activity assay described by Hamann et al. (2019). All measurements were performed in the presence of 2 mM of the individual nucleotide using a VICTOR Nivo Multimode Microplate Reader (PerkinElmer).

Table S1. Data collection and refinement statistics.

Data collection	CF1	CF2	CF3	CF4	CF5
Space group	$P2_12_12_1$	$P2_12_12_1$	$P2_12_12_1$	$P2_1$	$P2_12_12_1$
a (Å)	64.3	65.9	66.7	69.4	74.7
b (Å)	75.5	77.4	95.3	72.6	113.7
c (Å)	154.4	148.9	124.8	70.3	191.7
β (°)	90.0	90.0	90.0	93.3	90.0
X-ray source	P13, PETRA III, DESY	P13, PETRA III, DESY	P14, PETRA III, DESY	P14, PETRA III, DESY	P13, PETRA III, DESY
Resolution range (Å)	77.22 – 1.95 (2.05 – 1.95)	74.45 – 1.85 (1.95 – 1.85)	45.55 – 2.10 (2.20 – 2.10)	70.15 – 2.50 (2.60 – 2.50)	48.90 – 2.60 (2.71 – 2.60)
No. of unique reflections	55604	65564	46827	23946	50939
Completeness (%)	100.0 (99.9)	99.7 (99.8)	99.4 (99.4)	98.5 (98.7)	99.6 (99.7)
R_{merge} (%)	7.4 (133.5)	6.6 (109.9)	5.3 (114.4)	7.8 (66.1)	6.9 (93.0)
Average I/σ(I)	15.97 (2.08)	11.45 (1.84)	14.83 (1.58)	12.16 (1.92)	17.33 (1.83)
Redundancy	9.37 (9.75)	4.55 (4.64)	4.54 (4.65)	3.16 (3.07)	5.04 (5.10)
$CC_{1/2}$	99.9 (81.0)	99.8 (67.8)	99.9 (63.3)	99.7 (79.3)	99.9 (72.6)
Wilson B ($Å^2$)	46.62	45.42	55.89	55.35	66.75
Refinement					
Resolution (Å)	42.53 – 1.95 (1.98 – 1.95)	68.69 – 1.85 (1.88 – 1.85)	45.55 – 2.10 (2.14 – 2.10)	70.15 – 2.50 (2.60 – 2.50)	48.90 – 2.60 (2.65 – 2.60)
No. of reflections	55587	65546	46795	23930	50847
R_{work} (%)	20.00 (32.3)	19.79 (34.9)	22.41 (34.1)	20.81 (32.4)	22.22 (38.1)
R_{free} (%)	21.78 (34.6)	21.20 (36.0)	24.44 (34.6)	25.80 (38.1)	25.04 (40.8)
Molecules per asymmetric unit	1	1	1	1	2
Total number of atoms	5782	5850	5611	5022	10938
Protein residues	700	694	688	656	1375
Water molecules	190	319	192	4	116
r.m.s. deviations					
Bond length (Å)	0.004	0.011	0.009	0.009	0.004
Bond angles (°)	0.66	1.23	1.06	1.06	0.54
Mean B-factors ($Å^2$)	54.35	49.22	61.67	61.61	78.70
Ramachandran statistics					
favoured (%)	96.84	97.97	98.24	95.81	96.41
allowed (%)	3.02	2.03	1.76	3.73	3.37
outliers (%)	0.14	0.00	0.00	0.47	0.22
PDB accession code	6rm8	6rm9	6rma	6rmb	6rmc

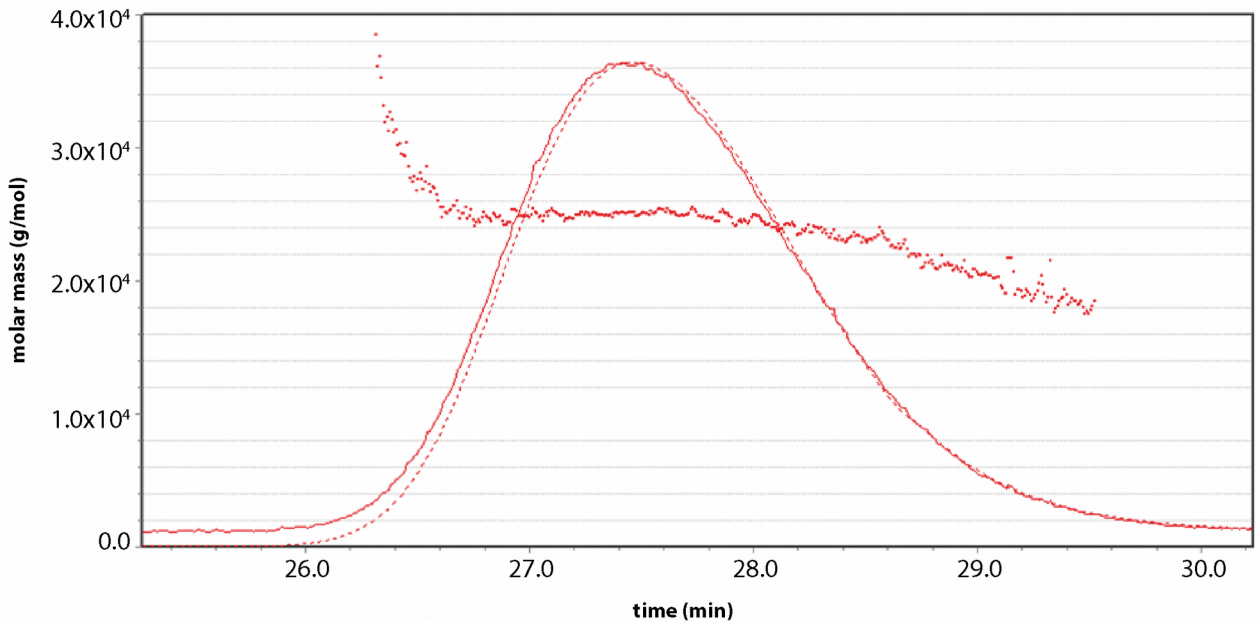

Fig. S1. MALS measurements of scSpp2$_{10\text{-}185}$

The determined molecular weight represented as dots is plotted against the time. UV-absorption and light scattering are shown as solid and dashed lines, respectively. The determined molecular weight of the protein within the UV Absorption peak is 2.453e+4 g/mol, corresponding to monomeric scSpp2$_{10\text{-}185}$.

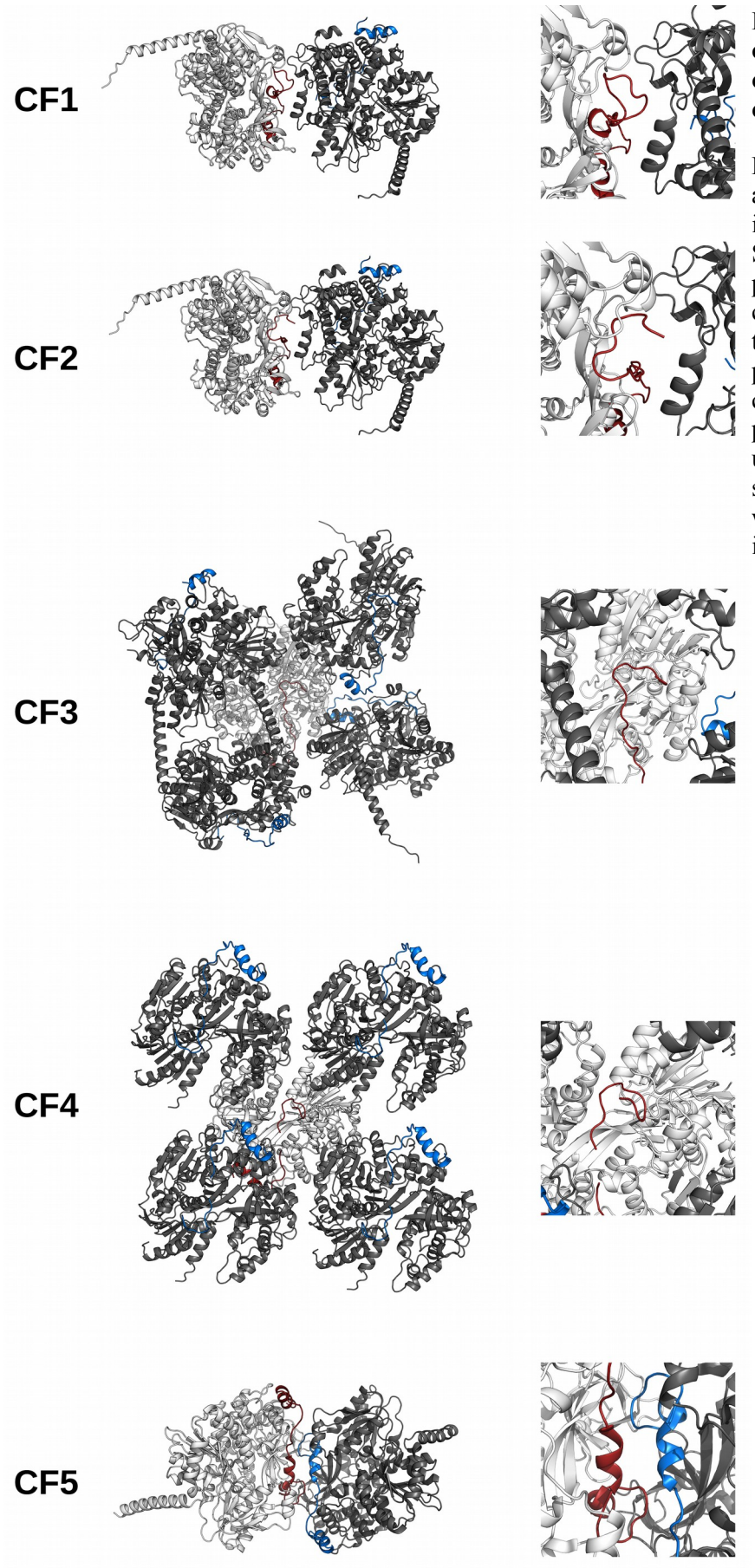

Fig. S2. Crystal contact overview of the C-terminal part of the ctSpp2 G-patch in the different crystal forms.

Prp2-Spp2 complexes are depicted as cartoon models. Prp2 is shown in different shades of gray and Spp2 either in red or blue. The left panels show an overview of the closest symmetry-based complexes to the C-terminal part of the G-patch. The right panels display a close-up view of the C-terminal part of the G-patch. CF1 and CF5 undergo crystal contacts with symmetry-related molecules, whereas CF2, CF3 and CF4 are not involved in crystal contacts.

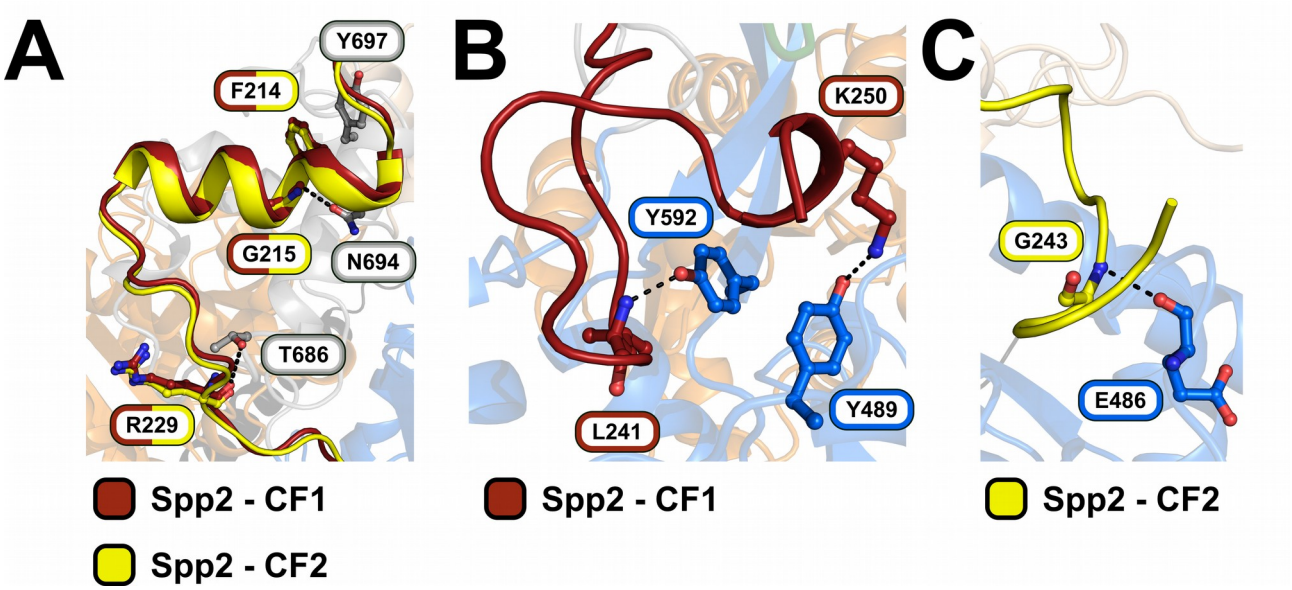

Fig. S3. Hydrogen bonds between ctSpp2$_{G\text{-}patch}$ and ctPrp2

(A) Additionally to the hydrophobic interactions, the N-terminal part of the G-patch is only involved in two further polar interactions and a π-π-stacking. **(B)** ctSpp2$_{G\text{-}patch}$ interacts via hydrogen bonding with two tyrosines of ctPrp2 in conformation 1. **(C)** In conformation 2 ctSpp2$_{G\text{-}patch}$ is only involved in one polar interaction with ctPrp2.

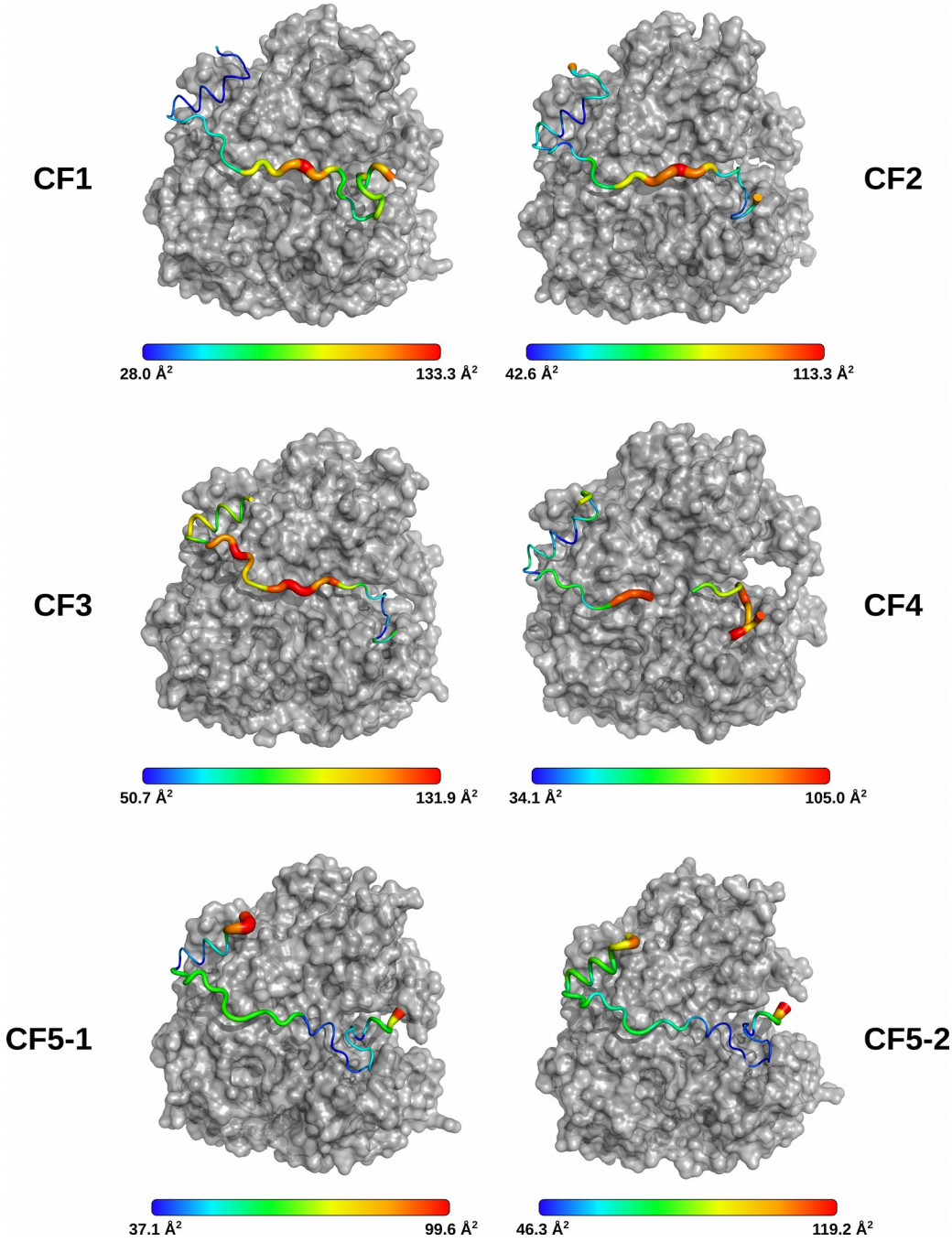

Fig S4. *B*-factors distribution of ctSpp2

The overview representation of the *B*-factors of ctSpp2 shows increased *B*-factor values for the linker connecting the N-terminal α-helix with the C-terminal hydrophobic stretch, highlighting the flexibility of this region. *B*-factor values are not elevated in CF5 due to crystal contacts.

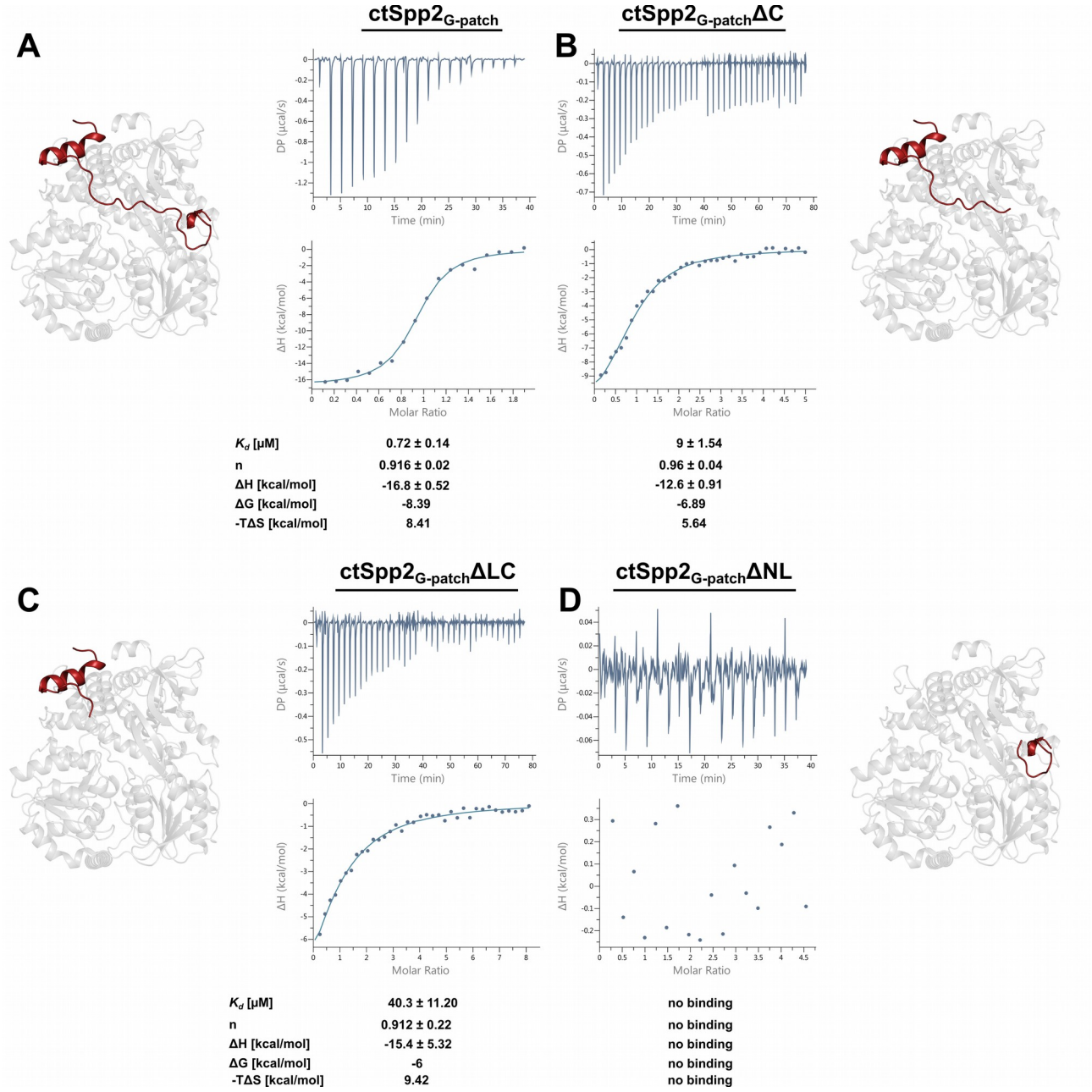

Fig. S5. ITC measurments of ctSpp2$_{G\text{-}patch}$ truncations

In order to test the influence of the different regions of ctSpp2$_{G\text{-}patch}$ on the binding towards ctPrp2, the interaction of ctPrp2 with different ctSpp2$_{G\text{-}patch}$ truncations was assessed via ITC. **(A)** ctSpp2$_{G\text{-}patch}$ binds ctPrp2 with a K_d of 0.72 µM. **(B)** The ctSpp2$_{G\text{-}patch}$ lacking the C-terminal stretch (ctSpp2$_{G\text{-}patch}$ΔC) exhibits a K_d of 9 µM. **(C)** The construct lacking the linker and C-terminal region, thus only containing the N-terminal helix (ctSpp2$_{G\text{-}patch}$ΔLC), shows a further 4-fold decrease in affinity (K_d= 40.3 µM). **(D)** The C-terminal stretch alone (ctSpp2$_{G\text{-}patch}$ΔNL) is not able of binding with ctPrp2.

A

	Conformation 1 (CF1)		Conformation 2 (CF2)	
	Phi	Psi	Phi	Psi
Gly215	-65.93	-38.22	-71.83	-35.65
Gly223	95.43	11.15	93.09	12.24
Gly226	90.20	2.53	88.45	-3.95
Gly230	87.30	149.42	70.61	163.06
Gly243	63.06	36.44	-60.49	158.88
Gly245	82.9	-142.61	76.28	-5.27

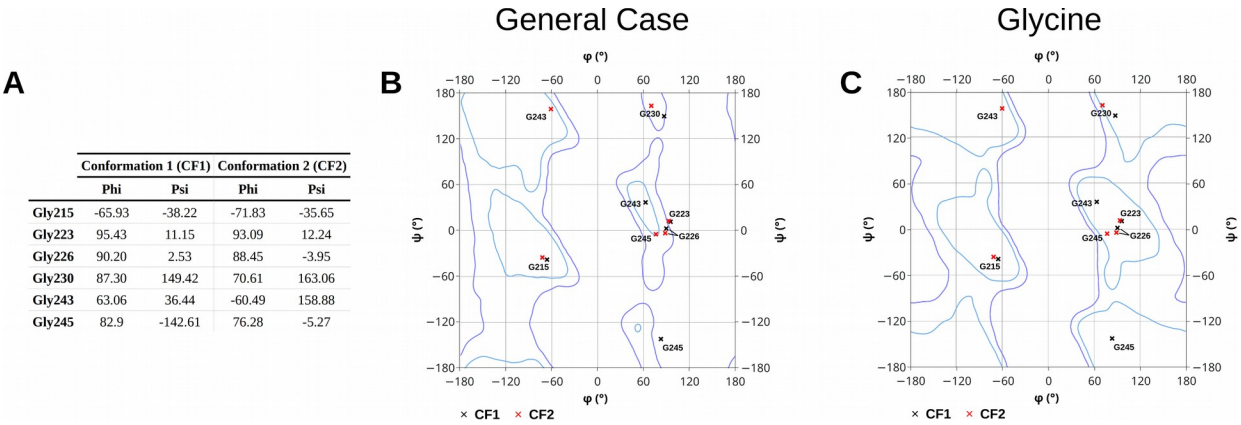

Fig. S6. Mainchain analysis of ctSpp2 glycines

(A) List of psi and phi angles of all glycines in the ctSpp2 G-patch. CF1 is used exemplary for conformation 1 and CF2 for conformation 2. **(B)** Ramachandran plot of ctSpp2 G-patch glycines depicted on favored (light blue) and allowed (dark blue) boundaries for all residues except glycine and proline. **(C)** Ramachandran plot of ctSpp2 G-patch glycines depicted on favored (light blue) and allowed (dark blue) boundaries for glycine.

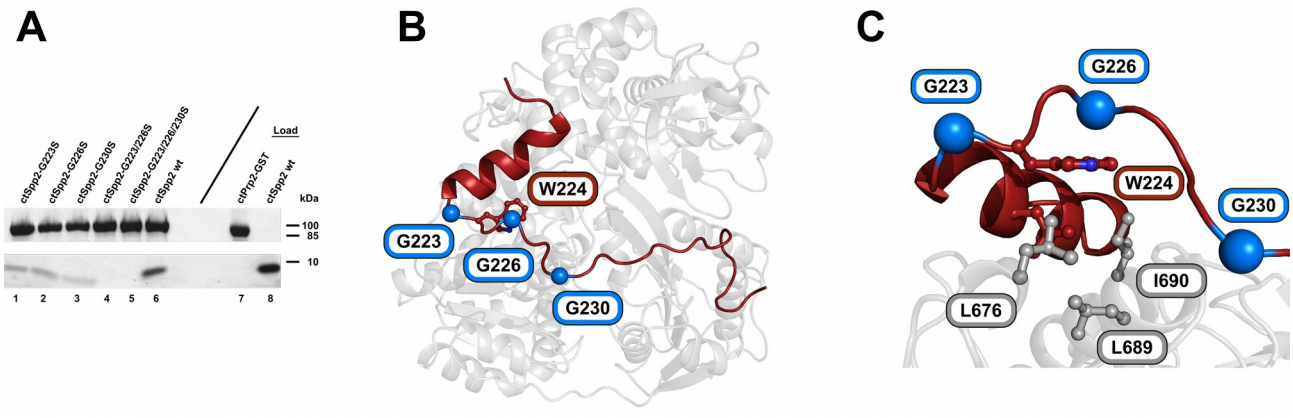

Fig. S7. GST pulldown experiments of key ctSpp2 G-patch glycine residues

Key glycine residues of the ctSpp2 G-patch motif have been mutated to serine and the binding towards ctPrp2 has been analyzed via GST pulldown experiments. **(A)** Single point mutants G223S (lane 1), G226 (lane 2) and G230 (lane 3) show significantly reduced binding to ctPrp2 compared with wildtype ctSpp2 (lane 6). Mutations of two (lane 4) or three (lane 5) glycines completely abolish the interaction with ctPrp2. **(B)** ctSpp2 glycines 223, 226 and 230 exhibit conformations only favored for glycines in all ctPrp2-ctSpp2 crystal structures and are involved in sharp kinks of the polypeptide chain. **(C)** Glycine 226 is involved in a CH/π interaction with tryptophane 224, which is stacked between this glycine and hydrophobic residues of ctPrp2 (L676, L689 and I690) in a conformation similar to the one observed in tryptophane-cage miniproteins.

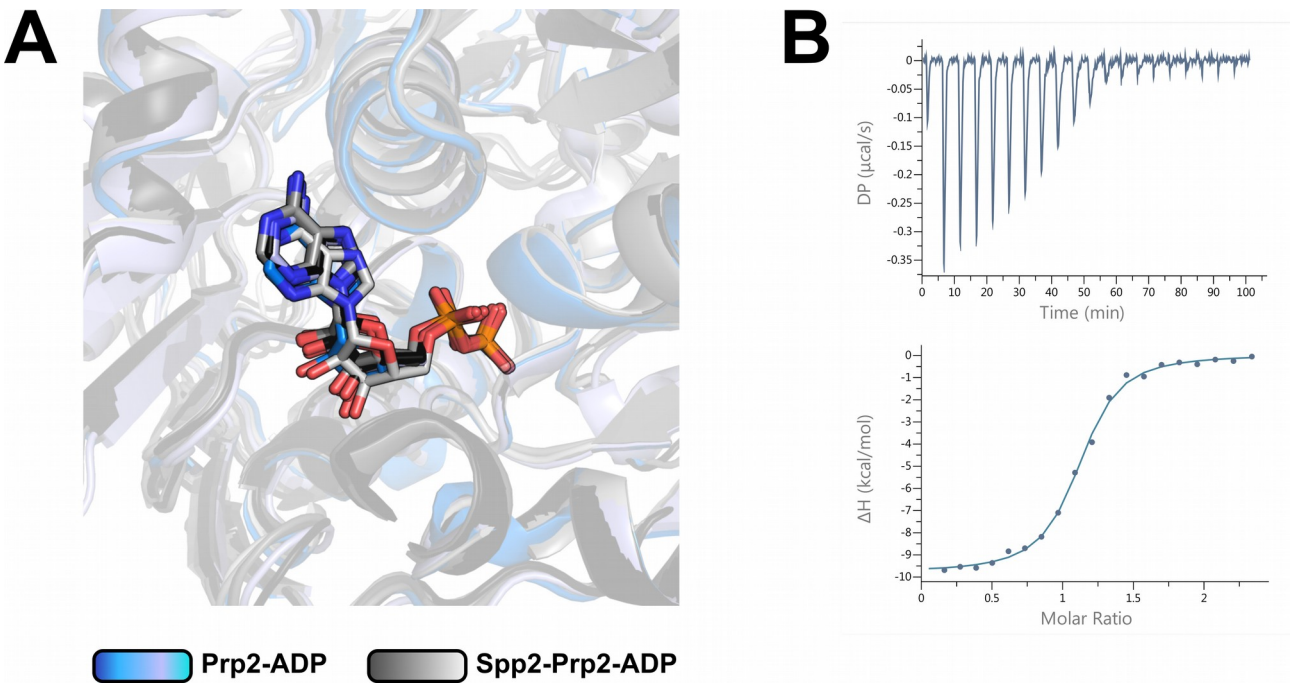

Fig. S8. ADP binding in Prp2-ADP and Spp2-Prp2-ADP complexes

(A) Prp2 is depicted as a semi-transparent cartoon model, the bound ADP is shown as a stick model. Prp2-ADP complex structures are displayed in different shades of gray and Spp2-Prp2-ADP structures in different shades of blue. The nucleotide binding site of Prp2 is not altered by the binding of the Spp2 G-patch, leading to an almost identical binding of the ADP in all Prp2-ADP and Spp2-Prp2-ADP structures. **(B)** Isothermal titration calorimetry measurements of ADP binding to Prp2 in presence of a two fold molar excess of Spp2 G-patch. A dissociation constant (K_d) of 172 ± 21.3 nM was determined (n= 1.08 ± 0.0089, ΔH= -9.83 ± 0.168 kcal/mol, ΔG= -9.23 kcal/mol). This value closely resembles the *Kd* of the ADP binding to Prp2 in absence of Spp2 G-patch (*Kd*= 179 nM), which was published by Schmitt el al. (2018) (2). The upper panel shows the thermograms and the lower panel shows the fit.

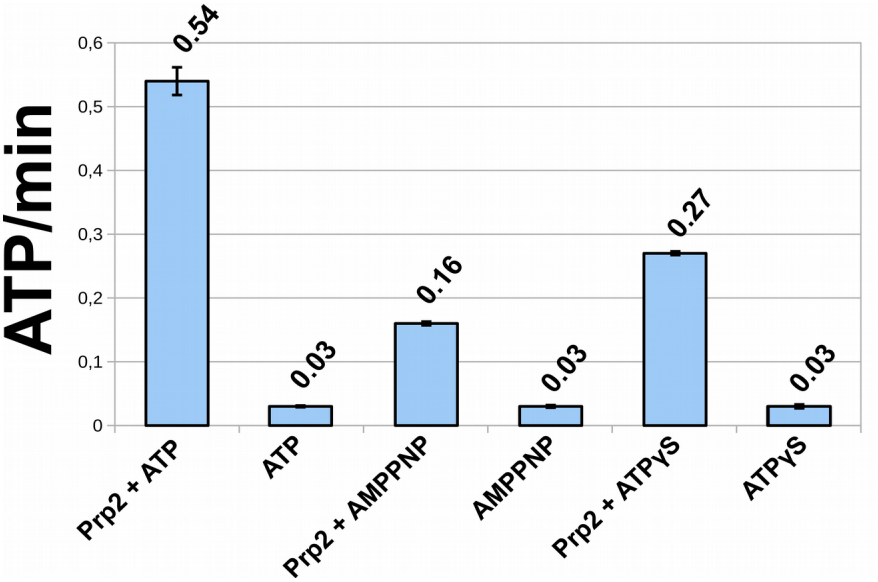

Fig. S9. ATPase activity of Prp2 in presence of ATP analogs AMPPNP and ATPγS

Neither crystallization nor binding experiments with Prp2 could be performed in presence of ATP analogs AMPPNP and ATPγS since for both nucleotides an ATPase activities were observed. The ATPase activity of Prp2 in the presence of the different nucleotides was tested using the ATPase activity assays described in Hamann et al. (2019) (15) using a concentration of 2 mM of the individual nucleotides for each measurement. Error bars represent the standard deviations (N=3).

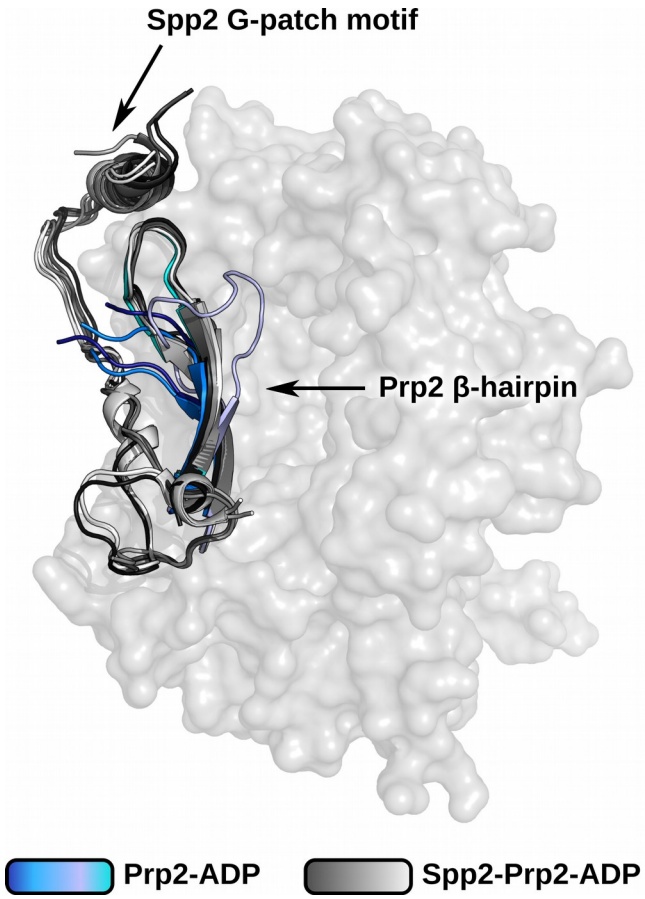

Fig. S10. Binding of Spp2 stabilized β-hairpin conformation

The overall structure of Prp2 is depicted as a semi-transparent surface model. The OB-fold domain was omitted for clarity reasons. Spp2 G-patch and the β-hairpin are displayed as cartoon models. Cartoon models shown in different shades of blue correspond to Prp2-ADP complex structures and models in different shades of gray represent Spp2-Prp2-ADP structures. While the β-hairpin exhibits multiple conformations in the different Prp2-ADP complex structures, the binding of Spp2 seems to stabilize one of these conformations in all Prp2-Spp2-ADP structures.

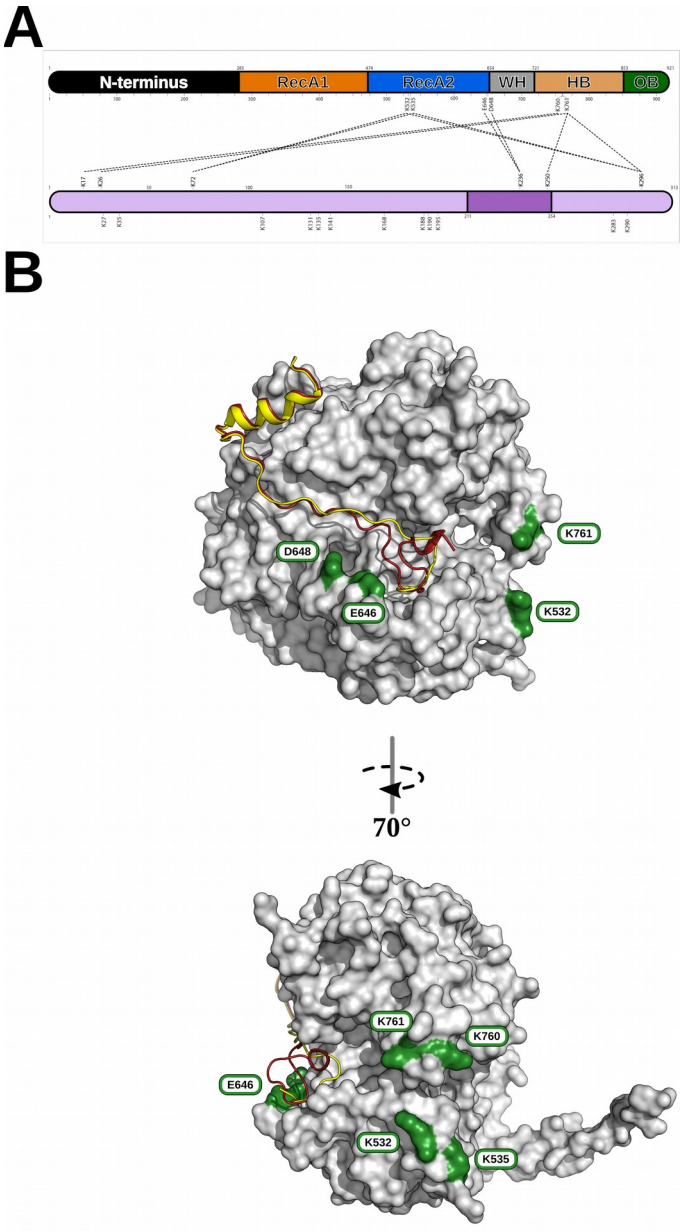

Fig. S11. Overview of cross-links between ctSpp2 and ctPrp2

(A) Map of ctSpp2-ctPrp2 cross-links. ctPrp2 is represented as the upper with coloring as in Figure 2 and ctSpp2 as the lower bar (length of bar not up to scale). Intermolecular cross-links are indicated by dashed lines between the corresponding residues. **(B)** ctPrp2 is depicted as a surface model in gray and the two alternative ctSpp2 conformations are displayed as cartoon models in red (conformation 1) and yellow (conformation 2). Cross-linked residues of ctPrp2 are highlighted in green and labeled accordingly.

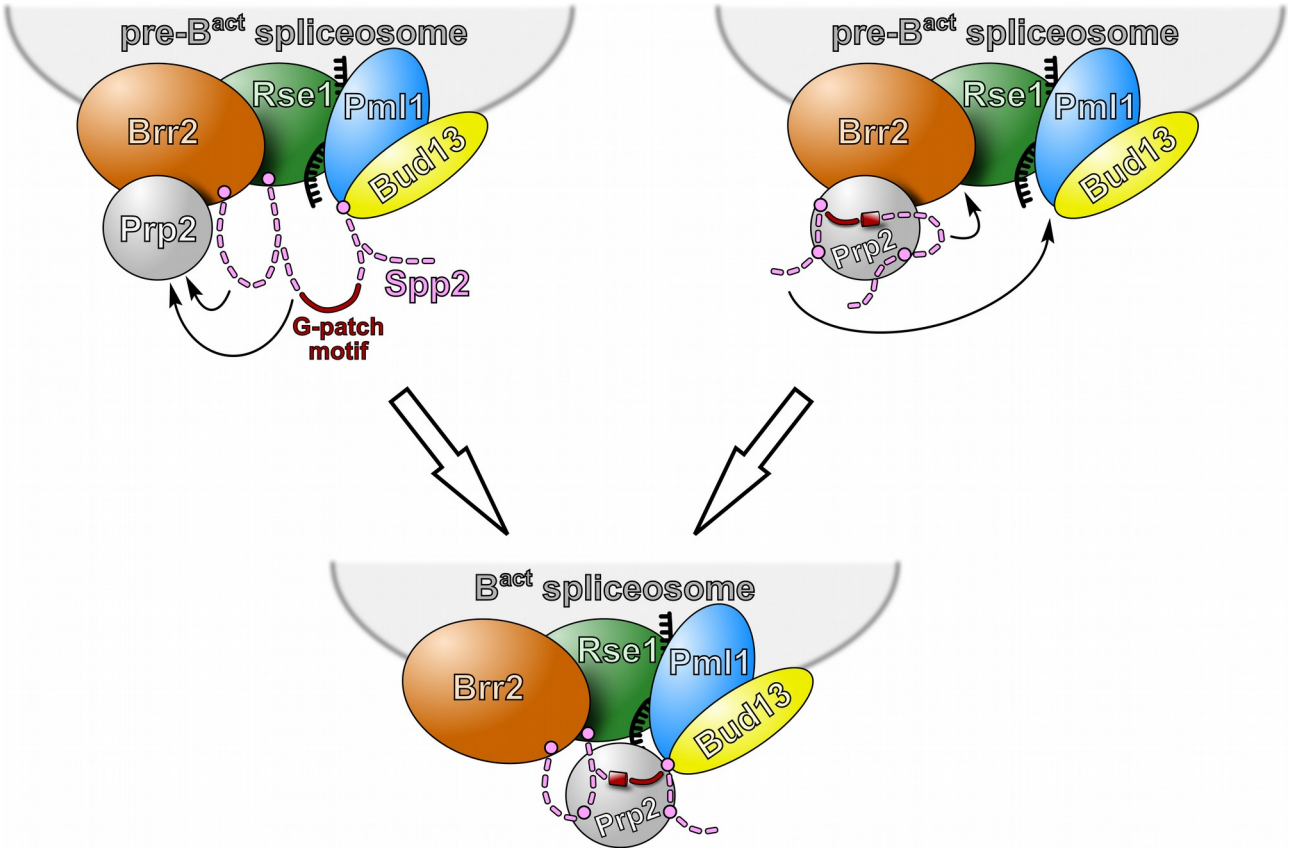

Fig. S12. Potential role of Spp2 in positioning Prp2 after recruitment to spliceosome

Prp2 might be recruited to the spliceosome via an interaction with Brr2 independently of the presence of Spp2. This would require a further correct positioning of Prp2 to its target site in order to interact with the pre-mRNA (black) and fulfill its function. Spp2 might play the role of repositioning Prp2. Is Spp2 already associated to the spliceosome at the functional site of Prp2, it might recognize the nearby Prp2 and thereby place Prp2 at its target site. If Prp2 interacts with Brr2 pre-loaded with Spp2, the G-patch protein might interact with the spliceosomal factors Brr2 (orange), Rse1 (green), Pml1 (blue) and Bud13 (yellow) and thereby reposition Prp2. In either scenario, Spp2 would guarantee the right positioning of Prp2 in order for the DEAH-box ATPase to interact with the pre-mRNA and remodel the B^{act}-spliceosome.

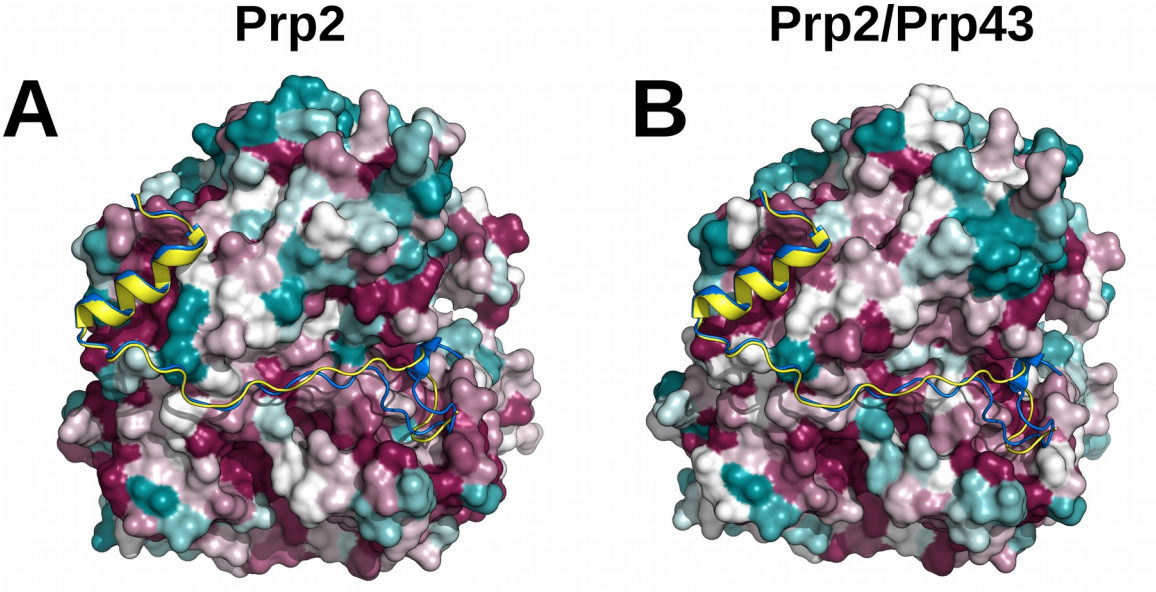

Fig. S13. Sequence conservation of Prp2 and Prp43

(A) The surface model of Prp2 is colored by sequence conservation using an alignment of Prp2 from *C. thermophilum*, *S. cerevisiae*, *H. sapiens*, *M. musculus*, *N. crassa* and *D. rerio,* with conserved and variable residues in purple and green, respectively. Residues of Prp2 interacting with the N-terminal α-helix and the C-terminal end of ctSpp2 G-patch are conserved. **(B)** The surface model of Prp2 is colored by sequence conservation using an alignment of Prp2 from *C. thermophilum*, *S. cerevisiae* and *H. sapiens* together with Prp43 from the same organisms. Prp43 shows the same conservation for the interaction sites with the N-terminal and C-terminal ends.

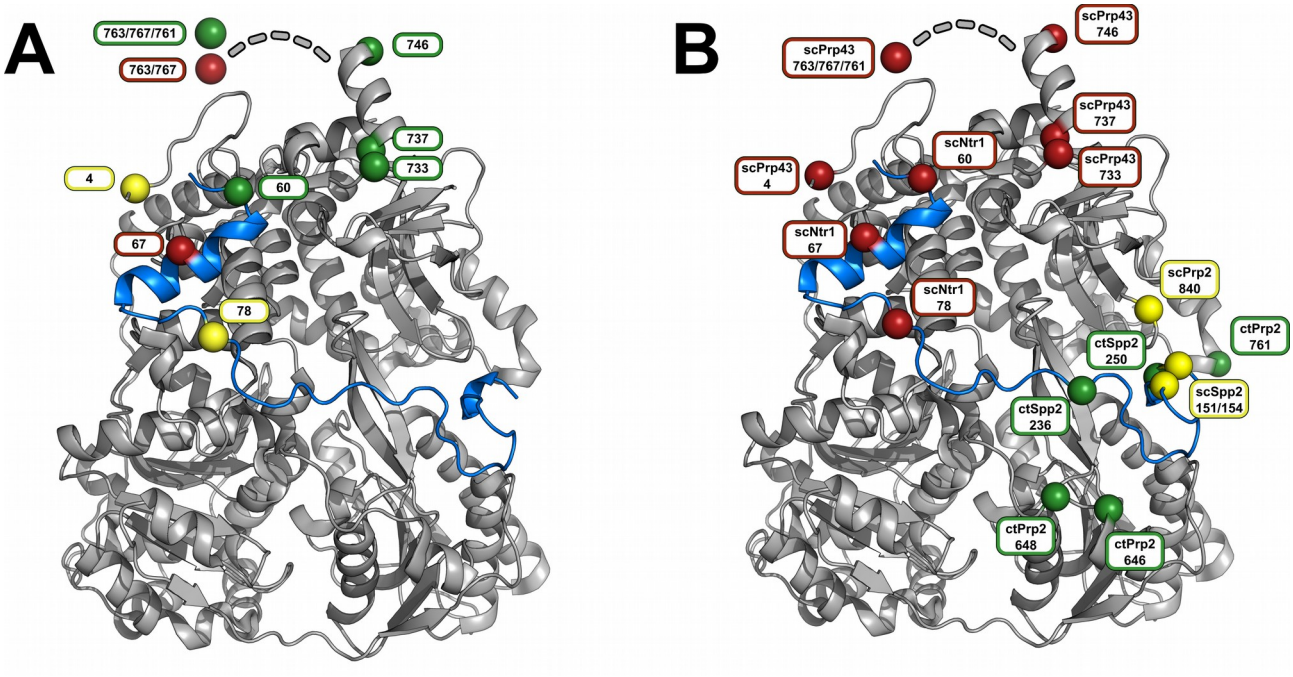

Fig. S14. Overview of scNtr1 and scPrp43 cross-links

(A) *Saccharomyces cerevisiae* Prp43 (scPrp43) is depicted as a gray cartoon model and *Saccharomyces cerevisiae* Ntr1 (scNtr1) was modeled as a blue cartoon model onto the scPrp43 structure assuming a similar binding as Spp2 to Prp2. Cross-link pairs identified by Christian et al. (2014) (14) between Ntr1 and Prp43 are colored in the same color and labeled accordingly. The found cross-links are in a feasible distance for an interaction mode of Ntr1 with Prp43 similar to the Spp2-Prp2 complex. **(B)** Overview of all known DEAH-box ATPase cross-links with its G-patch interaction partners. Cross-links between *Saccharomyces cerevisiae* Prp43 (scPrp43) and *Saccharomyces cerevisiae* Ntr1 (scNtr1) are shown in red (14), *Saccharomyces cerevisiae* Prp2 (scPrp2) and *Saccharomyces cerevisiae* Spp2 (scSpp2) in yellow (16), *Chaetomium thermophilum* Prp2 (ctPrp2) and *Chaetomium thermophilum* Spp2 (ctSpp2) in green.

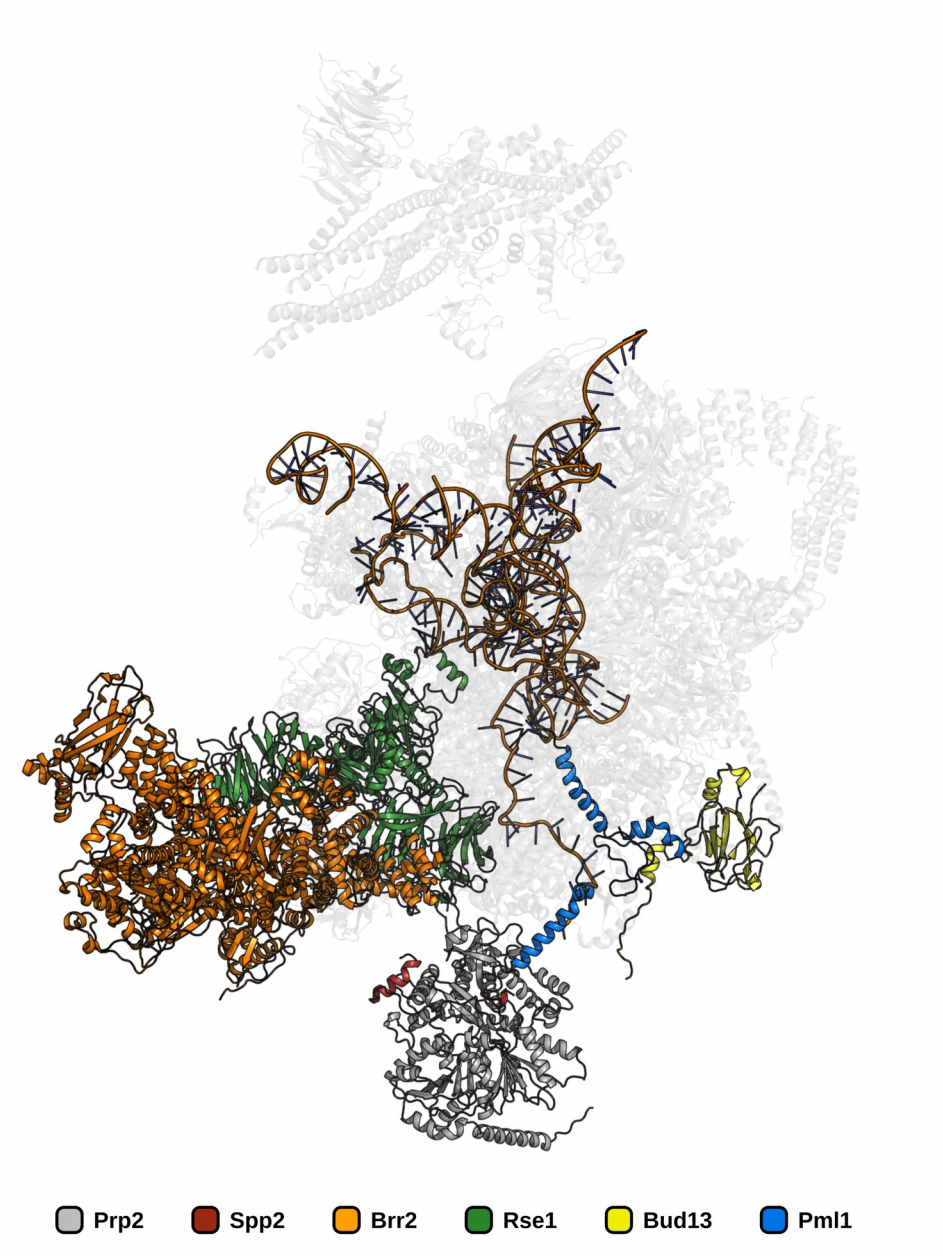

Fig. S15. Prp2-Spp2 complex in the spliceosomal B^{act} complex

The B^{act} spliceosome is depicted as a cartoon model. Spliceosomal factors not found to cross-link with Prp2 or Spp2 by Rauhut et al. (2016) (16) are shown as gray semi-transparent cartoon models. The Prp2-Spp2 complex structure was superimposed on the scPrp2 model of the B^{act} complex in order to estimate the position of the Spp2 G-patch in this spliceosomal complex.

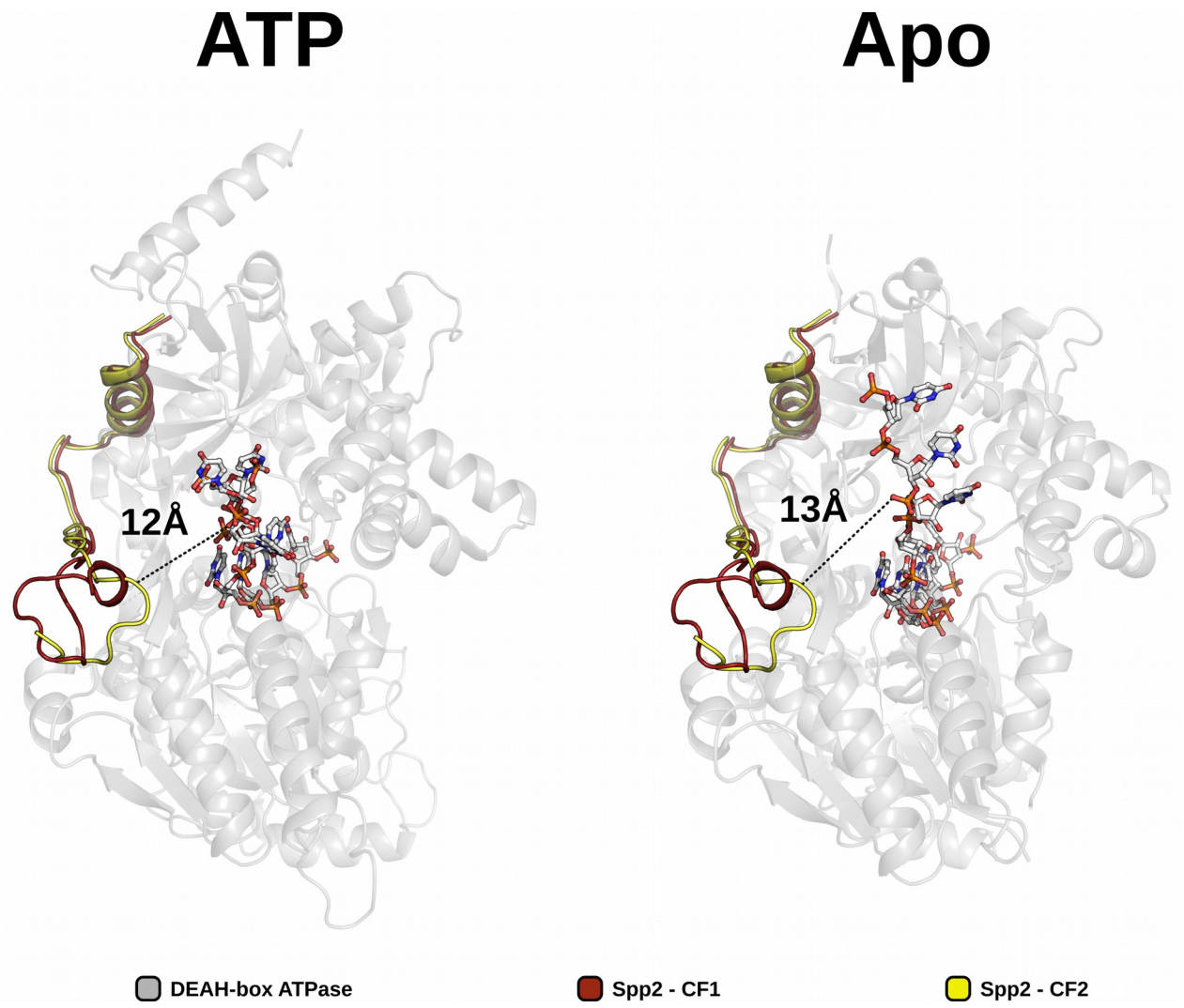

Fig. S16. Distance between the C-terminal end of the Spp2 G-patch and bound RNA

The position of the Spp2 G-patch in the ATP and Apo states was modeled by a superposition of the Prp2 RecA2 domain on the RecA2 domain of Prp43 (ATP) (17) and Prp22 (Apo) (15). In both states the closest distance of the G-patch to the RNA ranges between 12Å and 13Å. This distance is too big to predict a direct interaction between the Spp2 G-patch and the RNA.

References:

1. S. F. Altschul, W. Gish, W. Miller, E. W. Myers, D. J. Lipman, Basic local alignment search tool. *Journal of Molecular Biology* **215**, 403–410 (1990).

2. A. Schmitt, F. Hamann, P. Neumann, R. Ficner, Crystal structure of the spliceosomal DEAH-box ATPase Prp2. *Acta Crystallogr D Struct Biol* **74**, 643–654 (2018).

3. M. Sattler, J. Schleucher, C. Griesinger, Heteronuclear multidimensional NMR experiments for the structure determination of proteins in solution employing pulsed field gradients. *Progress in Nuclear Magnetic Resonance Spectroscopy* **34**, 93–158 (1999).

4. F. Delaglio, *et al.*, NMRPipe: a multidimensional spectral processing system based on UNIX pipes. *J. Biomol. NMR* **6**, 277–293 (1995).

5. W. F. Vranken, *et al.*, The CCPN data model for NMR spectroscopy: development of a software pipeline. *Proteins* **59**, 687–696 (2005).

6. V. Ozenne, *et al.*, Flexible-meccano: a tool for the generation of explicit ensemble descriptions of intrinsically disordered proteins and their associated experimental observables. *Bioinformatics* **28**, 1463–1470 (2012).

7. J. A. Marsh, V. K. Singh, Z. Jia, J. D. Forman-Kay, Sensitivity of secondary structure propensities to sequence differences between alpha- and gamma-synuclein: implications for fibrillation. *Protein Sci.* **15**, 2795–2804 (2006).

8. W. Kabsch, XDS. *Acta Crystallogr. D Biol. Crystallogr.* **66**, 125–132 (2010).

9. A. J. McCoy, *et al.*, Phaser crystallographic software. *J Appl Crystallogr* **40**, 658–674 (2007).

10. P. D. Adams, *et al.*, PHENIX: a comprehensive Python-based system for macromolecular structure solution. *Acta Crystallogr. Sect. D-Biol. Crystallogr.* **66**, 213–221 (2010).

11. P. Emsley, B. Lohkamp, W. G. Scott, K. Cowtan, Features and development of Coot. *Acta Crystallogr. D Biol. Crystallogr.* **66**, 486–501 (2010).

12. V. B. Chen, *et al.*, MolProbity: all-atom structure validation for macromolecular crystallography. *Acta Crystallogr. D Biol. Crystallogr.* **66**, 12–21 (2010).

13. C. Schmidt, H. Urlaub, iTRAQ-labeling of in-gel digested proteins for relative quantification. *Methods Mol. Biol.* **564**, 207–226 (2009).

14. H. Christian, R. V. Hofele, H. Urlaub, R. Ficner, Insights into the activation of the helicase Prp43 by biochemical studies and structural mass spectrometry. *Nucleic Acids Res.* **42**, 1162–1179 (2014).

15. F. Hamann, M. Enders, R. Ficner, Structural basis for RNA translocation by DEAH-box ATPases. *Nucleic Acids Res.* (2019) https:/doi.org/10.1093/nar/gkz150.

16. R. Rauhut, *et al.*, Molecular architecture of the Saccharomyces cerevisiae activated spliceosome. *Science* **353**, 1399–1405 (2016).

17. M. J. Tauchert, J.-B. Fourmann, R. Lührmann, R. Ficner, Structural insights into the mechanism of the DEAH-box RNA helicase Prp43. *eLife* **6**, e21510 (2017).